Experimental simulation of anyonic fractional statistics with an NMR quantum-information processor

Guanru Feng,[1,2,3] Guilu Long,[1,2] and Raymond Laflamme[3,4,*]
[1]*Department of Physics, Tsinghua University, Beijing 100084, China*
[2]*State Key Laboratory of Low-dimensional Quantum Physics, Tsinghua University, Beijing 100084, China*
[3]*Institute for Quantum Computing and Department of Physics, University of Waterloo, Waterloo, Ontario, Canada N2L 3G1*
[4]*Perimeter Institute for Theoretical Physics, Waterloo, Ontario, Canada N2J 2W9*
(Received 29 October 2012; revised manuscript received 24 June 2013; published 7 August 2013)

Anyons have exotic statistical properties, fractional statistics, differing from bosons and fermions. They can be created as excitations of some Hamiltonian models. Here, we present an experimental demonstration of anyonic fractional statistics by simulating a version of the Kitaev spin-lattice model proposed by Han *et al.* [Phys. Rev. Lett. **98**, 150404 (2007)] using an NMR quantum-information processor. We use a seven-qubit system to prepare a six-qubit pseudopure state to implement the ground-state preparation and realize anyonic manipulations, including creation, braiding and anyon fusion. The anyonic braiding process is equivalent to two successive particle exchanges. We obtain a phase difference of $(0.52 \pm 0.01)\pi \times 2$ between the states with and without anyon braiding, which is different from the $\pi \times 2$ and $2\pi \times 2$ phase changes for fermions and bosons after two successive particle exchanges, and agrees with the prediction of the anyonic fractional statistics.

DOI: 10.1103/PhysRevA.88.022305 PACS number(s): 03.67.Lx, 05.30.Pr, 03.67.Pp

I. INTRODUCTION

In three-dimensional space, indistinguishable particles obey Fermi-Dirac statistics (fermions) or Bose-Einstein statistics (bosons). For both fermions and bosons, upon the exchange of two indistinguishable particles, the system wave function gains a π or 2π phase change. However, when restricted to two-dimensional space, particles appear to obey fractional statistics [1]. This means that when two indistinguishable particles in two-dimensional space are exchanged, the system wave function gains a statistical phase change, ranging continuously from 0 to 2π. Those quasiparticles are defined as anyons. Anyons can be grouped in Abelian and non-Abelian anyons. Abelian anyons are particles that realize one-dimensional representations of braid groups. In nature, Abelian anyons are believed to exist and be responsible for the fractional quantum Hall effect (FQH) [2–4]. Non-Abelian anyons are particles that behave as multidimensional representations of braid groups. They are critical in topological quantum computing, for example, in the Kitaev fault-tolerant quantum computation models [5,6]. Recently, the interest in anyons is enhanced by the developing field of quantum computing because of their potential ability to implement fault-tolerant quantum computing architecture.

Several theoretical schemes have been proposed to directly observe the fractional statistics associated with the anyon braiding motion [7–20]. These schemes are mainly grouped into two approaches: the first is proposed to be realized in FQH systems, and the second makes use of the Kitaev models. In FQH systems, it is difficult to directly observe anyonic fractional statistics, and to introduce or resolve individual anyons [21] when compared with the schemes using the Kitaev spin-lattice models. Experimental demonstrations in photon systems using the Kitaev spin-lattice models have been realized [22,23]. However, the anyons are not protected from local noise and there is no explicit particle interpretation of the excitations [15] because the background Hamiltonian vanishes in such photon systems. In contrast, the background Hamiltonian can be simulated in the nuclear magnetic resonance (NMR) systems.

In our work, an NMR quantum-information processor is used to demonstrate the anyon braiding scheme proposed by Han *et al.* [12] in the smallest Kitaev system utilizing six qubits. The six-body ground-state preparation, anyon excitations, and anyonic braiding operations are realized using a seven-qubit molecule in liquid-state NMR. By comparing the two final states, of which one is obtained after the anyon creation, braiding, and fusion processes while the other does not undergo such processes, the phase difference, which is mapped into a frequency change of NMR spectrum peaks in our experiment, can be observed.

II. KITAEV $K \times K$ SQUARE-LATTICE MODEL

The first Kitaev spin-lattice model [5] is a $k \times k$ square lattice on the torus, containing qubits on each of the bonds (Fig. 1) (here, we define the bonds as the minimal lines forming the lattice). The total number of qubits is $2k^2$. The spin lattice contains vertices and faces. A vertex v is the intersection of four bonds. A face f means the surface with boundary defined by four bonds. We can then define a Hamiltonian as

$$H_K = -\sum_v A_v - \sum_f B_f, \tag{1}$$

where

$$A_v = \Pi_{j \in \text{vertex}(v)} \sigma_j^x, \quad B_f = \Pi_{j \in \text{face}(f)} \sigma_j^z. \tag{2}$$

A_v (B_f) represents the four-body interactions belonging to the qubits which live on the vertex v (or the face f). For all the vertices and faces, the ground state $|\Psi_{\text{ground}}\rangle$ for the Hamiltonian H_K satisfies

$$A_v|\Psi_{\text{ground}}\rangle = |\Psi_{\text{ground}}\rangle, \quad B_f|\Psi_{\text{ground}}\rangle = |\Psi_{\text{ground}}\rangle. \tag{3}$$

*laflamme@iqc.ca

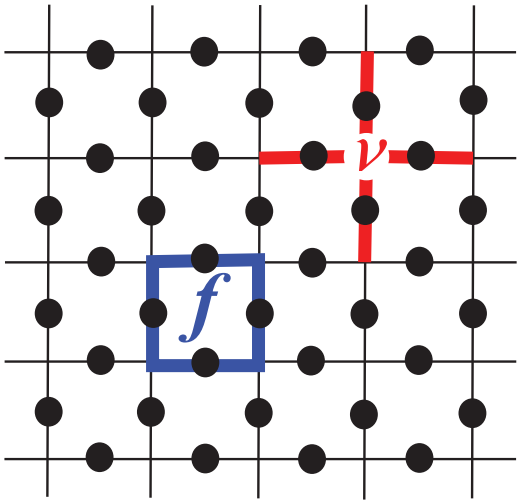

FIG. 1. (Color online) Illustration of the first Kitaev model. The first Kitaev spin-lattice model is a $k \times k$ square lattice on the torus. There is a qubit on each bond. The operators A_v and B_f act on the qubits of the vertex v and face f, respectively.

The ground states are fourfold degenerate. They form a protected subspace G:

$$G = \{|\xi\rangle \in N, A_v|\xi\rangle = |\xi\rangle, B_f|\xi\rangle = |\xi\rangle \text{ for all } v \text{ and } f\}. \tag{4}$$

N is the Hilbert space of the $2k^2$ qubits. This is the definition of the toric code, which is a special kind of stabilizer code [5]. A_v and B_f are its stabilizer operators. Because of the periodic boundary conditions, for each qubit j, σ_j^x and σ_j^z appear twice in different A_v's and B_f's. It can be easily obtained that

$$\Pi_v A_v = 1, \quad \Pi_f B_f = 1. \tag{5}$$

If a state does not satisfy several (for example, n) of the $A_v|\Psi\rangle = |\Psi\rangle$ and $B_f|\Psi\rangle = |\Psi\rangle$ constraints, it is an excited state with n elementary excitations (or quasiparticles). The relationships in Eq. (5) imply that the quasiparticles should appear in pairs.

If a σ_x operation is applied to a qubit, for example, qubit mm, in a ground state, the state wave function is $|\Psi\rangle_{mm} = X_{mm}|\Psi_{\text{ground}}\rangle$ (X_{mm} means the σ_x operation to qubit mm). It satisfies $B_{f1}|\Psi\rangle_{mm} = -|\Psi\rangle_{mm}$ and $B_{f2}|\Psi\rangle_{mm} = -|\Psi\rangle_{mm}$. $f1$ and $f2$ are the two faces next to qubit mm. That means two quasiparticles have been created at those particular locations. The two quasiparticles can be considered as two "defects" localized on faces $f1$ and $f2$. They are called m particles. Instead, if a σ_z operation is applied to a qubit, for example, qubit ee, in a ground state, the state wave function is $|\Psi\rangle_{ee} = Z_{ee}|\Psi_{\text{ground}}\rangle$ (Z_{ee} means the σ_z operation to qubit ee). It satisfies $A_{v1}|\Psi\rangle_{ee} = -|\Psi\rangle_{ee}$ and $A_{v2}|\Psi\rangle_{ee} = -|\Psi\rangle_{ee}$. This also means two quasiparticles occur. Here, $v1$ and $v2$ are the two neighboring vertices which are connected by the bond qubit ee lives on. The two quasiparticles can also be considered as "defects" localized on vertices $v1$ and $v2$. They are called e particles. The states with quasiparticles (excitations) are excited states. The creation operations of e and m particles are illustrated in Fig. 2(a).

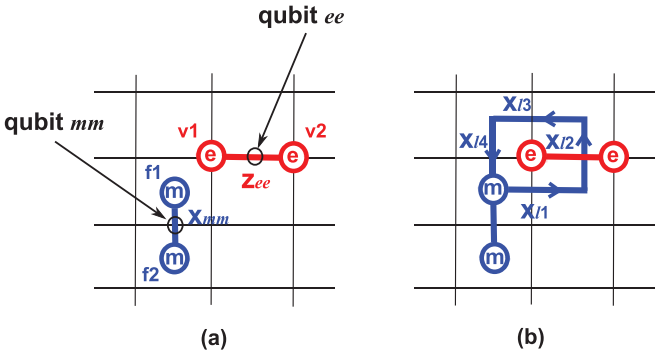

FIG. 2. (Color online) Illustration of anyon creation and braiding operations. (a) The creation of two m (e) anyons by the operation X_{mm} (Z_{ee}). X_{mm} means σ_x operation to qubit mm, and Z_{ee} means σ_z operation to qubit ee. The two m anyons are localized on faces $f1$ and $f2$. The two e anyons are localized on vertices $v1$ and $v2$. (b) The braiding motion of an m anyon around an e anyon by operations $X_{l1}X_{l2}X_{l3}X_{l4}$. Qubits $l1$, $l2$, $l3$, and $l4$ are the qubits along the braiding path.

Since two m (e) particles at the same site annihilate, the m (e) particle can be moved by applying σ_x (σ_z) operations along the path [Fig. 2(b)]. A braiding operation is to move an m (e) particle around an e (m) particle along a closed-circle path, which is equivalent to two successive particle exchanges [16]. For fermions and bosons, states do not change after two successive particle exchanges. For the m and e particles, it has been shown that after a braiding operation, the global state gains a $\frac{\pi}{2} \times 2$ phase change [5], which is different from fermions and bosons. Therefore, the m and e particles are anyons that obey fractional statistics.

III. SIX-QUBIT KITAEV SPIN-LATTICE MODEL AND THE EXPERIMENTAL SCHEME

The minimum amount of qubits needed to implement the smallest version of the periodic Kitaev model for anyon braiding operations is eight. However, by abandoning periodic condition, the spin-lattice model can be extended from a square lattice to any planar graph [24], and an anyonic model can be found with six qubits where we can demonstrate braiding statistics [12]. The graphic structure of the six-qubit model is shown in Fig. 3(a). The Hamiltonian of the system is

$$H_6 = -A_1 - A_2 - B_1 - B_2 - B_3 - B_4, \tag{6}$$

where

$$A_1 = \sigma_1^x\sigma_2^x\sigma_3^x, \quad A_2 = \sigma_3^x\sigma_4^x\sigma_5^x\sigma_6^x, \quad B_1 = \sigma_1^z\sigma_3^z\sigma_4^z,$$
$$B_2 = \sigma_2^z\sigma_3^z\sigma_5^z, \quad B_3 = \sigma_4^z\sigma_6^z, \quad B_4 = \sigma_5^z\sigma_6^z.$$

The ground state of the six-qubit Kitaev spin lattice is

$$|\Psi_{\text{ground}}\rangle = \tfrac{1}{2}(|000000\rangle + |111000\rangle + |110111\rangle + |001111\rangle). \tag{7}$$

Because the boundary conditions have changed, the ground state is not degenerate anymore. The ground state can be created from a six-qubit graph state shown in Fig. 3(b) [12]. A graph state is a type of multiqubit state represented by a graph

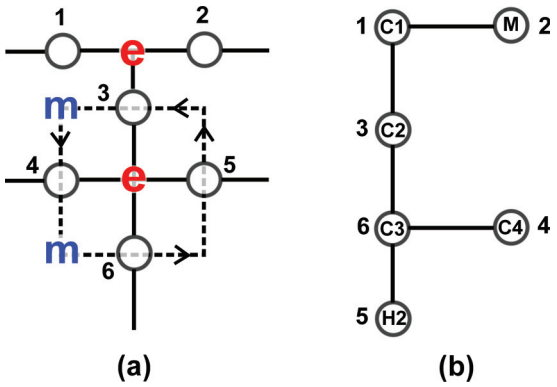

FIG. 3. (Color online) (a) The six-qubit Kitaev model and its braiding loop. A pair of m (e) anyons are created by the operation X_4 (Z_3) and the braiding operation is realized by $X_6X_5X_3X_4$. (b) The graph state that is equivalent under local unitary operations to the ground state of the Hamiltonian in (a). The corresponding qubits in the NMR spin system are also labeled at each vertex.

with the vertex set V and the edge set E, and is defined as

$$|G\rangle = \Pi_{(i,j)\in E} U_{i,j} |+\rangle^{\otimes V}, \tag{8}$$

where the operator $U_{i,j}$ is the controlled-σ_z operation between the qubits i and j, and $|+\rangle = \frac{1}{\sqrt{2}}(|0\rangle + |1\rangle)$. The six-qubit graph state corresponding to the graph in Fig. 3(b) is

$$|G_6\rangle = U_{1,2}U_{1,3}U_{3,6}U_{4,6}U_{5,6}|++++++\rangle. \tag{9}$$

The ground state of the six-qubit Kitaev spin lattice is

$$|\Psi_{\text{ground}}\rangle = O|G_6\rangle, \tag{10}$$

where $O = IHHHHI$, I is the identity operator, and H is the Hadamard operator. The $|\Psi_{\text{ground}}\rangle$ can be prepared by first preparing a six-qubit graph state $|G_6\rangle$, then implementing an O operation. This gives a method to prepare the ground state.

For the ground state of the six-qubit system in Fig. 3(a), if a σ_x operation is applied to qubit 4, a pair of m particles are created on its two neighboring faces, and if a σ_z is applied to qubit 3, a pair of e particles are created on its two neighboring vertices. By applying successive σ_x operations on qubits 6, 5, 3, and 4, one m particle moves in a loop around one e particle. After such a braiding operation, the global wave function will obtain a phase factor of -1. By observing this phase change, one can verify the fractional statistics of anyons.

Han *et al.* [12] give the basic circuit for ground-state preparation, anyon creation, anyon braiding, and anyon fusion. It should be noted that if one does the braiding operation to a state with a pair of e particles and a pair of m particles [Fig. 2(b)], the phase change after braiding is a global phase, which can not be observed in experiments directly. In the scheme proposed by Han *et al.* [12], the anyon creation step is realized by σ_x and $\sqrt{\sigma_z} = e^{i\frac{\pi}{4}} e^{-i\frac{\pi}{4}\sigma_z}$ instead of σ_x and σ_z. The σ_x operation creates a pair of m particles. The $\sqrt{\sigma_z}$ operation creates a superposition between the states with and without a pair of e particles. Therefore, after the anyon creation step, the state of the system is

$$|\Psi\rangle = \frac{1}{\sqrt{2}}(|\psi_1\rangle + |\psi_2\rangle), \tag{11}$$

where $|\psi_1\rangle$ is a state with a pair of m particles only, $|\psi_2\rangle$ is a state with a pair of m particles together with a pair of e particles. $|\psi_1\rangle$ will not change after a braiding procedure because no e particles exist. $|\psi_2\rangle$ will obtain a phase factor of $e^{i\delta}$ after a braiding procedure. Therefore, the total wave function becomes

$$|\Psi'\rangle = \frac{1}{\sqrt{2}}(|\psi_1\rangle + e^{i\delta}|\psi_2\rangle). \tag{12}$$

In this way, the phase change caused by braiding operation becomes a local phase factor in front of $|\psi_2\rangle$ and is observable in experiments.

The fusion operation is realized by applying $\sqrt{\sigma_z}$ and σ_x. In such case, the state of the system becomes $i\frac{1-e^{i\delta}}{2}|\Psi_{\text{ground}}\rangle + \frac{1+e^{i\delta}}{2}|\Psi_{\text{excited}}\rangle$ after the fusion operation, where $|\Psi_{\text{excited}}\rangle = \sigma_z|\Psi_{\text{ground}}\rangle$. For the m and e particles, the statistical phase change $\delta = \frac{\pi}{2} \times 2$. Thus, the state after fusion is $|\Psi_{\text{ground}}\rangle$. This means the e particle pair and the m particle pair are both fused.

In our experimental scheme, $\sqrt{\sigma_z}^{-1}$ and σ_x operations are performed as the fusion step (Fig. 5). The state of the system is $\frac{1+e^{i\delta}}{2}|\Psi_{\text{ground}}\rangle + i\frac{1-e^{i\delta}}{2}|\Psi_{\text{excited}}\rangle$ after the fusion operation. With the statistical phase change $\delta = \frac{\pi}{2} \times 2$ introduced by a braiding operation, the state after the fusion step should be $|\Psi_{\text{excited}}\rangle$. Otherwise, if $\delta = 2n\pi$ $(n = 0,1,2,\ldots)$, the state after the fusion step should be $|\Psi_{\text{ground}}\rangle$. Therefore, by observing the difference between the state after the fusion step and the ground state, we can demonstrate the fractional statistics of anyons.

IV. EXPERIMENTAL IMPLEMENTATION

In our experiments, ^{13}C-labeled transcrotonic acid dissolved in d6 acetone was used. The methyl group (denoted as M) contains three hydrogen nuclei. M can be used as a spin-half nucleus after a gradient-based subspace selection [26]. Thus, the system contains seven qubits: H1, C1, M, C2, C4, H2, and C3. The natural NMR Hamiltonian of this system is as follows:

$$H_{\text{NMR}} = -\Sigma_{i=1}^{7} \pi \nu_i Z_i + \Sigma_{i<j,i=1}^{7} \frac{\pi J_{i,j}}{2} Z_i Z_j. \tag{13}$$

Here, Z is the Pauli matrix σ_z, ν_i is the chemical shift of the ith spin, and $J_{i,j}$ is the J-coupling constant between the ith and the jth spins. The molecule and its parameters are described in Fig. 4.

To implement the anyon braiding, we first prepared the molecule in the labeled pseudopure state with a deviation matrix [27] of the form $\rho_i = Z_{\text{H1}}\mathbf{0}_{\text{C1}}\mathbf{0}_{\text{M}}\mathbf{0}_{\text{C2}}\mathbf{0}_{\text{C4}}\mathbf{0}_{\text{H2}}\mathbf{0}_{\text{C3}}$ where $\mathbf{0} = |\mathbf{0}\rangle\langle\mathbf{0}|$, using the method in Ref. [26]. We chose H1 as the label qubit, and C1, M, C2, C4, H2, C3 as qubits 1, 2, 3, 4, 5, and 6, to match to Fig. 3(b), using the neighboring couplings for shortening the gate operations in implementation.

Figures 5 and 6 show the circuits for the experiments with and without anyonic manipulation, respectively. There is a part indicated as "measurement" from which one can observe the phase change from the spectrum of the probe qubit (C2). These two experiments illustrated in Figs. 5 and 6 were carried out for comparison.

	H_1	C_1	M	C_2	C_4	H_2	C_3
H_1	-4859.72	3.98	6.88	155.42	6.46	15.52	-1.74
C_1		-2997.12	127.16	41.62	7.02	6.36	1.46
M			-1300.94	-7.10	-0.94	-1.72	6.58
C_2				-25520.37	1.18	-0.66	69.66
C_4					-29462.76	3.72	72.16
H_2						-4078.11	161.00
C_3							-21584.71

T_2(s)	0.76±0.04	1.09±0.04	0.80±0.09	0.92±0.02	0.97±0.04	0.74±0.05	0.84±0.04
T_1(s)	3.2±0.1	4.6±1.1	2.4±0.1	4.6±0.8	7.7±1.4	3.3±0.1	4.8±0.9

FIG. 4. (Color online) Characteristics of the molecule of transcrotonic acid [26,28]. The chemical shifts (diagonal elements) and J-coupling constants (off-diagonal elements) are given in Hz. The spin-lattice and spin-spin relaxation times T_1 and T_2 are listed at the bottom. The chemical shifts are given with respect to reference frequencies of 700.13 MHz (hydrogens) and 176.05 MHz (carbons). The three hydrogen nuclei in the methyl form a spin-$\frac{3}{2}$ group M. After using a gradient-based subspace selection, this group acts in its spin-$\frac{1}{2}$ subspace [26]. Therefore, M can be used as a single qubit. We thus have seven qubits, including the two hydrogens and four carbons.

The wave functions of the labeled states (a), (b), (c), (d) in Fig. 5, and (f) in Fig. 6 are as follows (the label qubit stays in the state Z and is omitted in the following equations):

$$\begin{aligned}|\Psi_a\rangle &= \tfrac{1}{2}(|0_{C1}0_M0_{C2}0_{C4}0_{H2}0_{C3}\rangle + |1_{C1}1_M1_{C2}0_{C4}0_{H2}0_{C3}\rangle \\ &\quad + |1_{C1}1_M0_{C2}1_{C4}1_{H2}1_{C3}\rangle + |0_{C1}0_M1_{C2}1_{C4}1_{H2}1_{C3}\rangle) \\ &= |\Psi_{\text{ground}}\rangle, \end{aligned} \tag{14}$$

$$\begin{aligned}|\Psi_b\rangle &= \frac{1}{2}(|0_{C1}0_M0_{C2}1_{C4}0_{H2}0_{C3}\rangle + i|1_{C1}1_M1_{C2}1_{C4}0_{H2}0_{C3}\rangle \\ &\quad + |1_{C1}1_M0_{C2}0_{C4}1_{H2}1_{C3}\rangle + i|0_{C1}0_M1_{C2}0_{C4}1_{H2}1_{C3}\rangle) \\ &= X_{C4}\left(\frac{1}{\sqrt{2}}(e^{i\frac{\pi}{4}}|\Psi_{\text{ground}}\rangle + e^{-i\frac{\pi}{4}}|\Psi_{\text{excited}}\rangle)\right) \\ &= \frac{1}{\sqrt{2}}(|\psi_1\rangle + |\psi_2\rangle), \end{aligned} \tag{15}$$

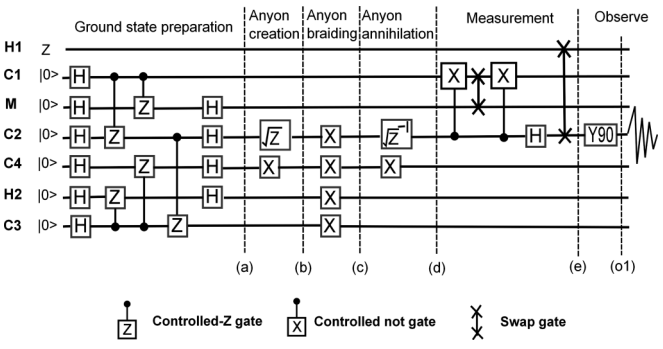

FIG. 5. The quantum network for the experiment with anyonic manipulation. H represents the Hadamard operation. $Z = \sigma_z$, $X = \sigma_x$. $Y90$ is the read pulse, $Y90 = e^{-i\frac{\pi}{4}\sigma_y}$.

$$\begin{aligned}|\Psi_c\rangle &= \frac{1}{2}(|0_{C1}0_M1_{C2}0_{C4}1_{H2}1_{C3}\rangle + i|1_{C1}1_M0_{C2}0_{C4}1_{H2}1_{C3}\rangle \\ &\quad + |1_{C1}1_M1_{C2}1_{C4}0_{H2}0_{C3}\rangle + i|0_{C1}0_M0_{C2}1_{C4}0_{H2}0_{C3}\rangle) \\ &= X_{C4}\left(\frac{1}{\sqrt{2}}(e^{i\frac{\pi}{4}}|\Psi_{\text{ground}}\rangle - e^{-i\frac{\pi}{4}}|\Psi_{\text{excited}}\rangle)\right) \\ &= \frac{1}{\sqrt{2}}(|\psi_1\rangle - |\psi_2\rangle), \end{aligned} \tag{16}$$

$$\begin{aligned}|\Psi_d\rangle &= \frac{i}{2}(|0_{C1}0_M0_{C2}0_{C4}0_{H2}0_{C3}\rangle - |1_{C1}1_M1_{C2}0_{C4}0_{H2}0_{C3}\rangle \\ &\quad + |1_{C1}1_M0_{C2}1_{C4}1_{H2}1_{C3}\rangle - |0_{C1}0_M1_{C2}1_{C4}1_{H2}1_{C3}\rangle) \\ &= iZ_{C2}|\Psi_{\text{ground}}\rangle = i|\Psi_{\text{excited}}\rangle, \end{aligned} \tag{17}$$

$$\begin{aligned}|\Psi_f\rangle &= \tfrac{1}{2}(|0_{C1}0_M0_{C2}0_{C4}0_{H2}0_{C3}\rangle + |1_{C1}1_M1_{C2}0_{C4}0_{H2}0_{C3}\rangle \\ &\quad + |1_{C1}1_M0_{C2}1_{C4}1_{H2}1_{C3}\rangle + |0_{C1}0_M1_{C2}1_{C4}1_{H2}1_{C3}\rangle) \\ &= |\Psi_{\text{ground}}\rangle. \end{aligned} \tag{18}$$

In the experiment with anyonic manipulation, $|\Psi_a\rangle$ is obtained after the ground-state preparation. It is the ground state of the six-qubit Kitaev model. After anyon creation, the wave function of the state is $|\Psi_b\rangle$. After anyon braiding, $|\Psi_b\rangle$ is transformed to $|\Psi_c\rangle$. $|\Psi_b\rangle$ and $|\Psi_c\rangle$ are the superpositions of $|\psi_1\rangle$ and $|\psi_2\rangle$. $|\psi_1\rangle$ is a state with a pair of m particles. $|\psi_2\rangle$ is a state with a pair of e particles and a pair of m particles. Due to the e anyons present in $|\psi_2\rangle$, it has a phase change acquired when the m particle braiding around the e particle. This causes the difference between $|\Psi_b\rangle$ and $|\Psi_c\rangle$. After anyon annihilation, the state goes to the excited state $|\Psi_d\rangle$. As a comparison, there is no anyonic manipulation part in the experiment illustrated in Fig. 6. Since the ground-state preparation procedure is the same as the experiment with anyonic manipulation, the state $|\Psi_f\rangle$ equals $|\Psi_a\rangle$.

The "measurement" part is designed in such a way that the state $|\Psi_d\rangle$ is transformed to $|\Psi_e\rangle$ and $|\Psi_f\rangle$ goes to $|\Psi_g\rangle$, where

$$\begin{aligned}|\Psi_e\rangle &= \frac{i\sqrt{2}}{2}(|0_{C1}0_M1_{H1}0_{C4}0_{H2}0_{C3}\rangle \\ &\quad + |1_{C1}1_M1_{H1}1_{C4}1_{H2}1_{C3}\rangle), \end{aligned} \tag{19}$$

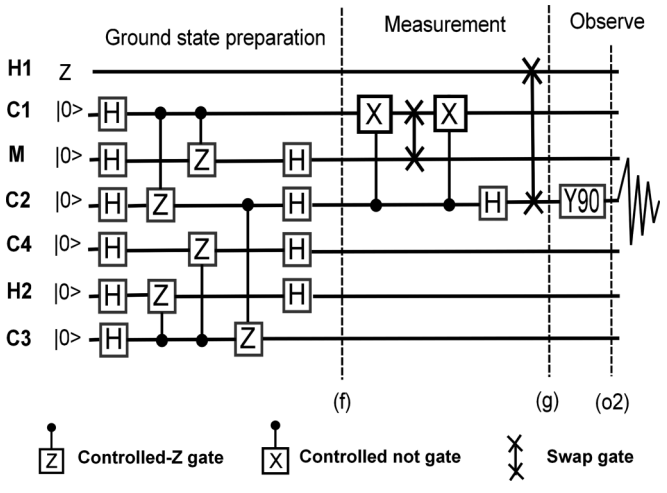

FIG. 6. The quantum network for the experiment without anyonic manipulation. It serves as a comparison with the experiment in Fig. 5.

$$|\Psi_g\rangle = \frac{\sqrt{2}}{2}(|0_{C1}0_M0_{H1}0_{C4}0_{H2}0_{C3}\rangle + |1_{C1}1_M0_{H1}1_{C4}1_{H2}1_{C3}\rangle). \quad (20)$$

It should be noted that at the end of the "measurement" part, the states of qubits H1 and C2 are exchanged via a swap gate. Therefore, after the "measurement" part, C2 becomes the label qubit in the state Z, and it is used as the probe qubit in the "observe" part. The state $|\Psi_g\rangle$ is almost the same as $|\Psi_e\rangle$, except that the qubit H1 is in state $|0\rangle$ in $|\Psi_g\rangle$ (the global phase is ignored).

In NMR experiments, we can detect the states of the qubits through measuring the free induction decay (FID) signal $S(t)$, which is the time-varying current signal induced by the rotating bulk magnetization. We have

$$S(t) \propto \mathrm{tr}[\rho(t)\Sigma_k(X_k + iY_k)e^{-t/T^*_{2,k}}]. \quad (21)$$

Here, $\rho(t) = U(t)\rho_0U^\dagger(t)$, where ρ_0 is the density matrix of the state that needs to be measured and $U(t) = e^{-itH_{\mathrm{NMR}}}$. $T^*_{2,k}$ is the effective transverse relaxation time of spin k. By doing Fourier transform to $S(t)$, the NMR spectrum can be obtained. Specifically, in our experiments, the detection is realized, as shown in the "observe" part in Figs. 5 and 6, by implementing a $\pi/2$ read pulse to the probe qubit, collecting the FID signals and then doing Fourier transform to get NMR spectra. After the read pulse, the deviation density matrices of the joint system (the probe qubit together with the remaining six qubits) for the marked states (o1) in Fig. 5 and (o2) in Fig. 6 are as follows:

$$\rho_{o1} = X_{C2} \otimes |\Psi_e\rangle\langle\Psi_e| = \begin{pmatrix} L & |\Psi_e\rangle\langle\Psi_e| \\ |\Psi_e\rangle\langle\Psi_e| & L \end{pmatrix}, \quad (22)$$

$$\rho_{o2} = X_{C2} \otimes |\Psi_g\rangle\langle\Psi_g| = \begin{pmatrix} L & |\Psi_g\rangle\langle\Psi_g| \\ |\Psi_g\rangle\langle\Psi_g| & L \end{pmatrix}. \quad (23)$$

Here, L is the 64×64 zero matrix. Equations (22) and (23) indicate that the information of the remaining six qubits is encoded in the coherent part of the reduced density matrix of the probe qubit. The coherent part is observable and can be directly measured in the NMR spectrum, which means the peaks of the probe qubit (C2) are associated with the states of the other spins. Therefore, by observation of C2, one can obtain information of the other six qubits (see Appendix).

To identify the state difference of H1 between $|\Psi_e\rangle$ and $|\Psi_g\rangle$, complete information of the six qubits is not necessary, and we only need to know the diagonal elements of their density matrices, which stand for the population distribution among the 64 eigenstates ($|0_{C1}0_M1_{H1}0_{C4}0_{H2}0_{C3}\rangle$, $|1_{C1}1_M1_{H1}1_{C4}1_{H2}1_{C3}\rangle$, $|0_{C1}0_M0_{H1}0_{C4}0_{H2}0_{C3}\rangle$, and $|1_{C1}1_M0_{H1}1_{C4}1_{H2}1_{C3}\rangle$ are 4 of them) of the six-qubit system. Therefore, we employ the method used in the previous work [28,29], extracting information of the other qubits by observing the probe qubit to reconstruct the deviation density matrix partially which is enough to measure the appropriate phase. To reconstruct the diagonal elements of the density matrices of the six qubits (M, H1, H2, C1, C3, C4), one observation of the probe qubit (C2) is enough for each experiment (see Appendix). For the experiment with anyonic manipulation, the observation is fulfilled by doing Fourier transform to the FID signals of the state ρ_{o1}, and for the experiment without anyonic manipulation the observation is fulfilled by doing Fourier transform to the FID signals of the state ρ_{o2}.

For the state $|\Psi_e\rangle$, by observing the probe qubit, a two-peak spectrum can be obtained. The intensity of the left peak in the spectrum is proportional to the population distribution on the eigenstate $|1_{C1}1_M1_{H1}1_{C4}1_{H2}1_{C3}\rangle$ while that of the right peak is proportional to the population distribution on $|0_{C1}0_M1_{H1}0_{C4}0_{H2}0_{C3}\rangle$ (see Appendix). For the state $|\Psi_g\rangle$, by observing the probe qubit, also a two-peak spectrum can be obtained. Similarly, the left peak in the spectrum corresponds to $|1_{C1}1_M0_{H1}1_{C4}1_{H2}1_{C3}\rangle$ while the right peak corresponds to $|0_{C1}0_M0_{H1}0_{C4}0_{H2}0_{C3}\rangle$. The frequency distance between the two left (right) peaks in the two spectra is $|J_{C2,H1}|$, corresponding to the state difference of H1 between $|\Psi_e\rangle$ and $|\Psi_g\rangle$. We conclude that the difference between the two spectra is caused by anyon braiding. Because m and e anyons do not obey integral statistics, after two successive exchangings in the experiment illustrated in Fig. 5, they give rise to a phase factor, which is mapped into a frequency change of peaks in our experiments (or to say a change in the population distribution among the 64 eigenstates). Thus, by implementing the "measurement" part we succeed in observing directly the anyonic phase change in relatively simple spectra.

It should be mentioned that the J-coupling constant between C2 and H2 $|J_{C2,H2}| = 0.66$ Hz is the smallest of the couplings between C2 and the other nuclei. $|J_{C2,H2}|$ can be resolved in our experiments, which means all the 64 peaks of C2 spectrum are resolved (Fig. 7). $|J_{C2,H1}| = 155.42$ Hz is the largest J-coupling constant of C2. Therefore the braiding-induced changes can be easily and explicitly observed in our experiments.

The gates used in the ground-state preparation were realized by combining single-qubit rotations and evolutions of the J-coupling constants between the neighboring qubits, while all the anyonic manipulations were realized by single-qubit rotations [30,31]. The pulses of single-qubit rotations along x and y axes were generated using the GRAPE algorithm [32] for H1 and H2, and were standard Isech-shaped rf pulses for M and C1–C4. The single-qubit rotations along the z axis were realized using the evolutions of the chemical shifts in the Hamiltonian of the spin system [33]. The J-coupling evolutions were realized by implementing refocusing pulses. We combined all the pulses using a custom-built software compiler, which numerically optimizes refocusing pulses and minimizes the errors due to undesired J-coupling evolutions [29,33]. The duration of the experiments shown in Figs. 6 and 5 was 195.1 and 250.2 ms, respectively.

V. EXPERIMENTAL RESULTS

The final results for the experiments are shown in Fig. 7. Figure 7(a) shows the superposed spectra between the simulated thermal state spectrum of C2 and the experimental pseudopure state spectrum. It shows the experimentally realized $|0_{C1}0_M0_{H1}0_{C4}0_{H2}0_{C3}\rangle$ peak (peak o). It should be mentioned that there is an antiphase peak (peak w) in Fig. 7(a). This antiphase peak was caused by the label qubit H1, which was in the Z state. Figure 7(b) displays the spectrum of the experiment without anyonic manipulation, and Fig. 7(c) displays the spectrum of the experiment with

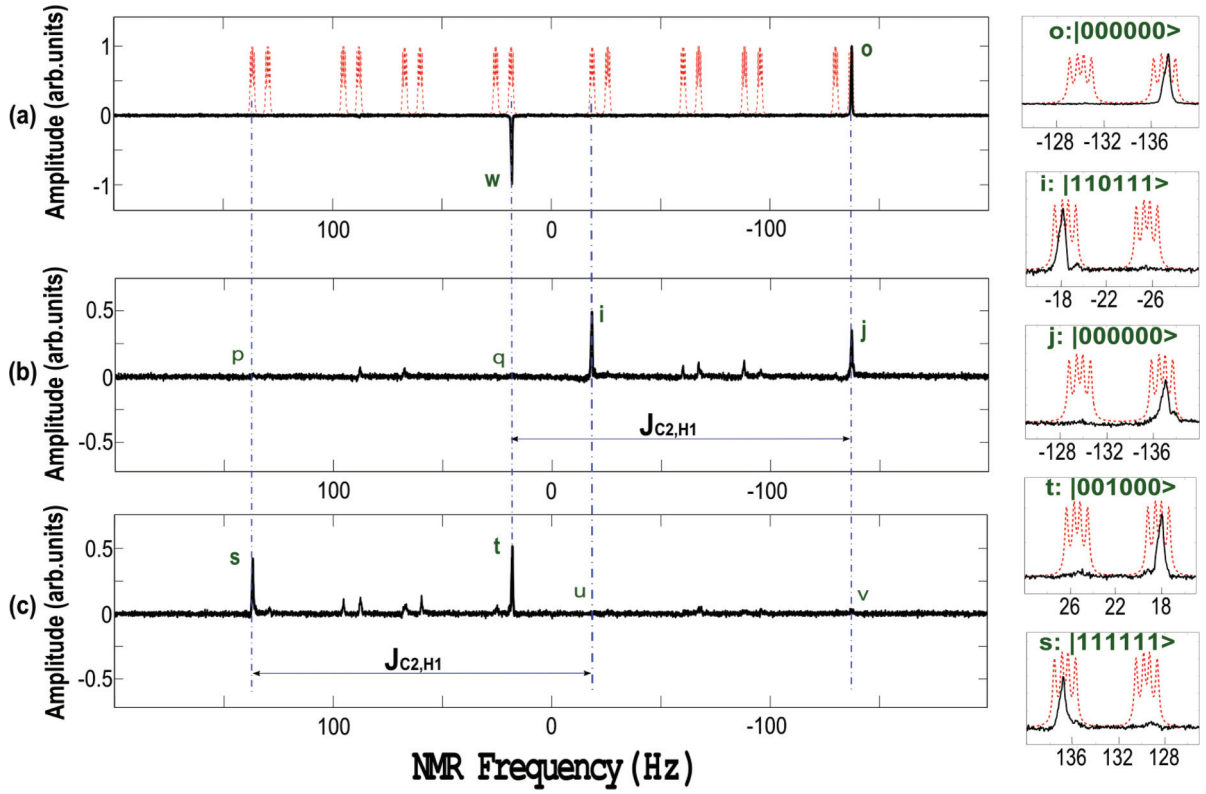

FIG. 7. (Color online) (a) The superposed spectra of the theoretical C2 thermal state spectrum (red dotted line) and the experimental pseudopure state spectrum (black solid line). There are 64 peaks in the thermal state spectrum, each corresponding to a computational basis state. (b) The experimental spectrum corresponding to the experiment in Fig. 6. It has two dominant peaks: i and j. (c) The experimental spectrum corresponding to the experiment in Fig. 5. It has two dominant peaks: s and t. The amplitude of peak o in the experimental pseudopure state spectrum in (a) is taken as reference to normalize the experimental signals shown in (b) and (c). On the right are the zoomed-in spectra for the peaks o, i, j, t, and s. The states which the experimental peaks correspond to are labeled on top of each zoomed-in spectrum. There is a $|J_{C2,H1}|$ distance between peaks i and s, j and t. p, q, u, and v are the small peaks that have the same frequencies as those of peaks s, t, i, and j, respectively.

anyonic manipulation, both generated by observing C2, whose deviation density matrix was X. Peaks i (-18.3 Hz), j (-137.2 Hz), s (137.1 Hz), and t (18.2 Hz) correspond to states $|1_{C1}1_M0_{H1}1_{C4}1_{H2}1_{C3}\rangle$, $|0_{C1}0_M0_{H1}0_{C4}0_{H2}0_{C3}\rangle$, $|1_{C1}1_M1_{H1}1_{C4}1_{H2}1_{C3}\rangle$, and $|0_{C1}0_M1_{H1}0_{C4}0_{H2}0_{C3}\rangle$, respectively. We obtain the intensities of these peaks via a spectral fitting procedure [29]. The sum intensity of the two dominant peaks, both in Figs. 7(b) and 7(c), is about 0.7, normalized using the intensity of peak o. More detailed, the intensities for peaks i, j, s and t are 0.41 ± 0.01, 0.30 ± 0.01, 0.31 ± 0.01, and 0.38 ± 0.01 (the error bars are estimated from the uncertainty of the fitting parameters), respectively. From the Eqs. (14)–(18), we can know that peak i and peak t originated from the same part $(|1_{C1}1_M0_{C2}1_{C4}1_{H2}1_{C3}\rangle + |0_{C1}0_M1_{C2}1_{C4}1_{H2}1_{C3}\rangle)$ of the ground state, and similarly peak j and peak s originated from the other part $(|0_{C1}0_M0_{C2}0_{C4}0_{H2}0_{C3}\rangle + |1_{C1}1_M1_{C2}0_{C4}0_{H2}0_{C3}\rangle)$ of the ground state. The fact peak t is slightly larger than peak s is consistent with the fact peak i is slightly larger than peak j.

There is a frequency difference which equals $|J_{C2,H1}|$ between peaks i and s, j, and t (Fig. 7), which was caused by the process of anyonic manipulation, demonstrating that after the braiding operation, the state with e and m anyons acquired an experimental phase change $\delta_{\text{expt}} = (\frac{\pi}{2} + \eta) \times 2$. Here, 2η is the deviation of the experimental phase change from $\frac{\pi}{2} \times 2$.

By doing simulations, we estimate that the intensity difference between peaks i and j and that between peaks s and t mainly arise from imperfect ground-state preparation and it has little influence on the anyonic braiding process (see the note in Ref. [34]). Thus, for an evaluation of the anyonic braiding process, we only focus on the imperfection of the braiding operation, which caused the deviation of the experimental phase change δ_{expt} from $\frac{\pi}{2} \times 2$. Let us assume that the experimentally realized labeled state (a) in Fig. 5 and labeled state (f) in Fig. 6 were

$$|\Psi_f{}'\rangle = |\Psi_a{}'\rangle = \alpha|\Psi_{\text{ground}}\rangle + \beta|\Psi_{\text{excited}}\rangle + \gamma|\Psi_{\text{error}}\rangle. \quad (24)$$

$\alpha|\Psi_{\text{ground}}\rangle$, $\beta|\Psi_{\text{excited}}\rangle$, and $\gamma|\Psi_{\text{error}}\rangle$ are all orthogonal to each other. The experimentally realized labeled state (g) in Fig. 6 was

$$\begin{aligned}|\Psi_g{}'\rangle = \frac{\sqrt{2}}{2}[&\alpha(|0_{C1}0_M0_{H1}0_{C4}0_{H2}0_{C3}\rangle \\ &+ |1_{C1}1_M0_{H1}1_{C4}1_{H2}1_{C3}\rangle) \\ &+ \beta(|0_{C1}0_M1_{H1}0_{C4}0_{H2}0_{C3}\rangle \\ &+ |1_{C1}1_M1_{H1}1_{C4}1_{H2}1_{C3}\rangle)] + \gamma|\Psi_{\text{error}}{}'\rangle. \quad (25)\end{aligned}$$

Here, $\gamma|\Psi_{\text{error}}{}'\rangle$ was transformed from $\gamma|\Psi_{\text{error}}\rangle$ via the part labeled "measurement" in Fig. 6, and it was responsible for the peaks other than peaks i, j, p, and q in Fig. 7(b).

From Eq. (25), we know that $|\alpha|^2$ is proportional to the population distribution on the eigenstates $|0_{C1}0_M0_{H1}0_{C4}0_{H2}0_{C3}\rangle$ and $|1_{C1}1_M0_{H1}1_{C4}1_{H2}1_{C3}\rangle$, and $|\beta|^2$ is proportional to the population distribution on the eigenstates $|0_{C1}0_M1_{H1}0_{C4}0_{H2}0_{C3}\rangle$ and $|1_{C1}1_M1_{H1}1_{C4}1_{H2}1_{C3}\rangle$. Therefore, $|\frac{\beta}{\alpha}|$ can be determined from the peak intensities (denoted as Γ) of the experimental spectrum shown in Fig. 7(b) (see Appendix). $|\frac{\beta}{\alpha}|$ depends on the sum of the intensities of peaks i and j, and the sum of p and q:

$$\left|\frac{\beta}{\alpha}\right| = \sqrt{\frac{\Gamma_p + \Gamma_q}{\Gamma_i + \Gamma_j}} = 0.18 \pm 0.09. \tag{26}$$

The experimentally realized labeled states (b), (c), (d), and (e) in Fig. 5 were

$$|\Psi_b{}'\rangle = \frac{\sqrt{2}}{2}[\alpha(|\psi_1\rangle + |\psi_2\rangle) + \beta e^{-i\frac{\pi}{2}}(|\psi_1\rangle - |\psi_2\rangle)] + \gamma X_{C4}\sqrt{Z_{C2}}|\Psi_{\text{error}}\rangle, \tag{27}$$

$$|\Psi_c{}'\rangle = \frac{\sqrt{2}}{2}[\alpha(|\psi_1\rangle + e^{i(\pi+2\eta)}|\psi_2\rangle) + \beta e^{-i\frac{\pi}{2}}(|\psi_1\rangle - e^{i(\pi+2\eta)}|\psi_2\rangle)] + \gamma X_{C4}\sqrt{Z_{C2}}|\phi_{\text{error}}\rangle, \tag{28}$$

$$\begin{aligned}|\Psi_d{}'\rangle &= ie^{i\eta}[(-\alpha\sin\eta - \beta\cos\eta)|\Psi_{\text{ground}}\rangle \\ &\quad + (\alpha\cos\eta - \beta\sin\eta)|\Psi_{\text{excited}}\rangle] + \gamma|\phi_{\text{error}}\rangle \\ &= ie^{i\eta}[\alpha'|\Psi_{\text{ground}}\rangle + \beta'|\Psi_{\text{excited}}\rangle] + \gamma|\phi_{\text{error}}\rangle,\end{aligned} \tag{29}$$

$$\begin{aligned}|\Psi_e{}'\rangle = \frac{\sqrt{2}ie^{i\eta}}{2}[&\alpha'(|0_{C1}0_M0_{H1}0_{C4}0_{H2}0_{C3}\rangle \\ &+ |1_{C1}1_M0_{H1}1_{C4}1_{H2}1_{C3}\rangle) \\ &+ \beta'(|0_{C1}0_M1_{H1}0_{C4}0_{H2}0_{C3}\rangle \\ &+ |1_{C1}1_M1_{H1}1_{C4}1_{H2}1_{C3}\rangle)] + \gamma|\phi_{\text{error}}{}'\rangle.\end{aligned} \tag{30}$$

Here, $\eta = \frac{\delta_{\text{expt}}}{2} - \frac{\pi}{2}$, $\alpha' = -\alpha\sin\eta - \beta\cos\eta$, $\beta' = \alpha\cos\eta - \beta\sin\eta$. $\gamma|\phi_{\text{error}}\rangle$ was transformed from $\gamma|\Psi_{\text{error}}\rangle$ via anyonic manipulation, and became $\gamma|\phi_{\text{error}}{}'\rangle$ after the "measurement" part. $\gamma|\phi_{\text{error}}{}'\rangle$ was responsible for the peaks other than s, t, u, and v in Fig. 7(c). The difference between $|\Psi_b{}'\rangle$ and $|\Psi_c{}'\rangle$ was the phase difference $\delta_{\text{expt}} = \pi + 2\eta$ for $|\psi_2\rangle$, caused by the braiding operation. $\alpha'|\Psi_{\text{ground}}\rangle$, $\beta'|\Psi_{\text{excited}}\rangle$, and $\gamma|\phi_{\text{error}}\rangle$ are all orthogonal to each other. Comparing Eqs. (24) and (29), we know that $|\Psi_{\text{ground}}\rangle$ and $|\Psi_{\text{excited}}\rangle$ compose a closed subspace upon the anyonic manipulation, which was confirmed in our experiments that the sum intensity of peaks i, j, p, and q approximately equals to that of peaks s, t, u, and v, with $\frac{\Gamma_i+\Gamma_j+\Gamma_p+\Gamma_q}{\Gamma_s+\Gamma_t+\Gamma_u+\Gamma_v} \approx 1.0$.

From Eq. (30), we know that, similar to $|\alpha|^2$ and $|\beta|^2$, $|\alpha'|^2$ is proportional to the population on the eigenstates $|0_{C1}0_M0_{H1}0_{C4}0_{H2}0_{C3}\rangle$ and $|1_{C1}1_M0_{H1}1_{C4}1_{H2}1_{C3}\rangle$, and $|\beta'|^2$ is proportional to the population on the eigenstates $|0_{C1}0_M1_{H1}0_{C4}0_{H2}0_{C3}\rangle$ and $|1_{C1}1_M1_{H1}1_{C4}1_{H2}1_{C3}\rangle$. Therefore, $|\frac{\beta'}{\alpha'}|$ can be determined from the experimental spectrum shown in Fig. 7(c) (see Appendix):

$$\left|\frac{\alpha'}{\beta'}\right| = \sqrt{\frac{\Gamma_u + \Gamma_v}{\Gamma_s + \Gamma_t}} = 0.24 \pm 0.06. \tag{31}$$

The error bars in Eqs. (26) and (31) are estimated from the uncertainty of the fitting parameters. Combining Eqs. (26) and (31), we can obtain

$$\tan\eta = \frac{|\frac{\alpha'}{\beta'}| - |\frac{\beta}{\alpha}|}{1 + |\frac{\beta}{\alpha}| * |\frac{\alpha'}{\beta'}|} = 0.06 \pm 0.03. \tag{32}$$

$\eta = 0.06 \pm 0.03 = (0.02 \pm 0.01)\pi$ and the phase change $\delta_{\text{expt}} = (\frac{\pi}{2} + \eta) \times 2 = (0.52 \pm 0.01)\pi \times 2$. This agrees with the prediction of the fractional statistics.

VI. DISCUSSION

The signal loss mainly came from the spin-spin relaxation and pulse imperfection. Through comparing the signal intensities of the simulation with and without the T_2 effects, we estimate that T_2 effects contributed to about 15% of the loss of signal. Comparing the experimental results (peak intensity $\sim$0.7) with the results of the simulation without T_2 effects (peak intensity $\sim$1), we estimate that imperfections of the implementation of rf pulses caused an additional approximate 15% signal loss.

Despite the signal loss, the phase factor, which was acquired during the anyonic braiding process, can still be extracted from the experimental spectra. The experimental deviation from the theoretically predicted value was mainly caused by imperfections of the experimental refocusing protocols and the implementation of rf pulses, and decoherence did not contribute much, which was checked by the numerical simulations with and without T_2 effects which both gave about 4% error, matching well with the experimental data.

VII. CONCLUSION

In summary, we demonstrated the anyonic fractional statistics, using a seven-qubit NMR system. We obtain a phase difference of $(0.52 \pm 0.01)\pi \times 2$ between the states with and without anyon braiding, which agrees with the prediction of the fractional statistics. This is a demonstration on topological quantum computing using nuclear spins. One advantage of our experimental scheme is that we can use the same technique to simulate a nine-qubit Kitaev spin model mentioned by Han *et al.* [12] using an NMR system with more spins, so that we can do a demonstration that anyonic operation is robust to different braiding paths and thus taking an important step towards showing the fault tolerance properties of the Kitaev model.

ACKNOWLEDGMENTS

We thank J.-F. Zhang for helpful discussions, and Industry Canada for support at the Institute for Quantum Computing. R.L. acknowledges support from CIFAR and NSERC. G.L. acknowledges support from the National Natural Science Foundation of China (Grant No. 10874098), and the National Basic Research Program of China (2009CB929402).

APPENDIX: PARTIAL STATE TOMOGRAPHY

We use the spectra obtained from the probe qubit C2 to partially reconstruct the density matrices of the remaining six qubits (C1, M, H1, C4, H2 and C3) [29,35]. We span the density matrices in Eqs. (22) and (23) as a sum of product operators, whose expansion coefficients can be directly related to the peak amplitudes in the spectra of the probe qubit [35]. Specifically, when considering the NMR observables $XZ^{\bar{n}_1}Z^{\bar{n}_2}Z^{\bar{n}_3}Z^{\bar{n}_4}Z^{\bar{n}_5}Z^{\bar{n}_6}$ $(\bar{n}_1,\ldots,\bar{n}_6 = 0,1)$, the relation between them and the peak intensities of the probe qubit can be expressed as

$$C = 2A \cdot P. \tag{A1}$$

C and P are column vectors, and A is an $n \times n$ matrix. The nth element of C, $C(n)$, is the coefficient related to the operator $XZ^{\bar{n}_1}Z^{\bar{n}_2}Z^{\bar{n}_3}Z^{\bar{n}_4}Z^{\bar{n}_5}Z^{\bar{n}_6}$ with the order of qubits C2, C1, M, H1, C4, H2, C3. The vector $\bar{n} = (\bar{n}_1,\bar{n}_2,\bar{n}_3,\bar{n}_4,\bar{n}_5,\bar{n}_6)$ is the six-digit binary representation of the integer $n-1$. The nth element of P, $P(n)$, is the intensity of the peak whose frequency is $\Sigma_{i=1}^{6}(-)^{\bar{n}_i-1}J_i/2$, where $J_1 = J_{\mathrm{C2,C1}}$, $J_2 = -J_{\mathrm{C2,M}}$, $J_3 = J_{\mathrm{C2,H1}}$, $J_4 = J_{\mathrm{C2,C4}}$, $J_5 = J_{\mathrm{C2,H2}}$, $J_6 = J_{\mathrm{C2,C3}}$. The elements of A are given by

$$A(k,m) = \Pi_{i=1}^{6}(-1)^{\bar{k}_i\bar{m}_i}. \tag{A2}$$

P can be obtained from one spectrum of the probe qubit. Thus, by one measurement of the probe qubit, we can have full knowledge of C, and reconstruct the diagonal elements of the density matrix of the remaining six qubits via linear combinations of $C(n)$. By simple calculations, we can also know that $P(n)$ is proportional to the nth diagonal element of the density matrix of the six qubits, which stands for the population distribution on the nth eigenstate of the six-qubit subsystem.

[1] F. Wilczek, Phys. Rev. Lett. **48**, 1144 (1982).
[2] D. C. Tsui, H. L. Stormer, and A. C. Gossard, Phys. Rev. Lett. **48**, 1559 (1982).
[3] R. B. Laughlin, Phys. Rev. Lett. **50**, 1395 (1983).
[4] D. Arovas, J. R. Schrieffer, and F. Wilczek, Phys. Rev. Lett. **53**, 722 (1984).
[5] A. Yu. Kitaev, Ann. Phys. (NY) **303**, 2 (2003).
[6] A. Yu. Kitaev, Ann. Phys. (NY) **321**, 2 (2006).
[7] L.-M. Duan, E. Demler, and M. D. Lukin, Phys. Rev. Lett. **91**, 090402 (2003).
[8] S. Das Sarma, M. Freedman, and C. Nayak, Phys. Rev. Lett. **94**, 166802 (2005).
[9] A. Stern and B. I. Halperin, Phys. Rev. Lett. **96**, 016802 (2006).
[10] P. Bonderson, A. Kitaev, and K. Shtengel, Phys. Rev. Lett. **96**, 016803 (2006).
[11] A. Micheli, G. K. Brennen, and P. Zoller, Nat. Phys. **2**, 341 (2006).
[12] Y.-J. Han, R. Raussendorf, and L.-M. Duan, Phys. Rev. Lett. **98**, 150404 (2007).
[13] C. Weeks, G. Rosenberg, B. Seradjeh, and M. Franz, Nat. Phys. **3**, 796 (2007).
[14] C. Zhang, V. W. Scarola, S. Tewari, and S. Das Sarma, Proc. Natl. Acad. Sci. USA **104**, 18415 (2007); J. Vidal, S. Dusuel, and K. P. Schmidt, arXiv:0801.4620; C. Zhang, V. W. Scarola, S. Tewari, and S. Das Sarma, arXiv:0801.4918; S. Dusuel, K. P. Schmidt, and J. Vidal, Phys. Rev. Lett. **100**, 177204 (2008).
[15] L. Jiang, G. K. Brennen, A. V. Gorshkov, K. Hammerer, M. Hafezi, E. Demler, M. D. Lukin, and P. Zoller, Nat. Phys. **4**, 482 (2008).
[16] G. K. Brennen and J. K. Pachos, Proc. R. Soc. A **464**, 1 (2008).
[17] M. Aguado, G. K. Brennen, F. Verstraete, and J. I. Cirac, Phys. Rev. Lett. **101**, 260501 (2008).
[18] G. Rosenberg, B. Seradjeh, C. Weeks, and M. Franz, Phys. Rev. B **79**, 205102 (2009).
[19] J. Q. You, X.-F. Shi, X. Hu, and F. Nori, Phys. Rev. B **81**, 014505 (2010).
[20] V. V. Ponomarenko and D. V. Averin, Phys. Rev. B **82**, 205411 (2010).
[21] F. Wilczek, Phys. World **19**, 22 (2006).
[22] J. K. Pachos, W. Wieczorek, C. Schmid, N. Kiesel, R. Pohlner, and H. Weinfurter, New J. Phys. **11**, 083010 (2009).
[23] C.-Y. Lu, W.-B. Gao, O. Gühne, X.-Q. Zhou, Z.-B. Chen, and J.-W. Pan, Phys. Rev. Lett. **102**, 030502 (2009).
[24] E. Dennis, A. Kitaev, A. Landahl, and J. Preskill, J. Math. Phys. **43**, 4452 (2002).
[25] L. M. K. Vandersypen and I. L. Chuang, Rev. Mod. Phys. **76**, 1037 (2005).
[26] E. Knill, R. Laflamme, R. Martinez, and C.-H. Tseng, Nature (London) **404**, 368 (2000).
[27] I. L. Chuang, N. Gershenfeld, M. G. Kubinec, and D. W. Leung, Phys. Eng. Sci. **454**, 447 (1998).
[28] J.-F. Zhang, M. Grassl, B. Zeng, and R. Laflamme, Phys. Rev. A **85**, 062312 (2012).
[29] A. M. Souza, J.-F. Zhang, C. A. Ryan, and R. Laflamme, Nat. Commun. **2**, 169 (2011).
[30] A. Barenco, C. H. Bennett, R. Cleve, D. P. DiVincenzo, N. Margolus, P. Shor, T. Sleator, J. A. Smolin, and H. Weinfurter, Phys. Rev. A **52**, 3457 (1995).
[31] L. M. K. Vandersypen, M. Steffen, M. H. Sherwood, C. S. Yannoni, G. Breyta, and I. L. Chuang, Appl. Phys. Lett. **76**, 646 (2000).
[32] N. Khaneja, T. Reiss, C. Kehlet, T. Schulte-Herbrüggen, and S. J. Glaser, J. Magn. Reson. **172**, 296 (2005).
[33] C. A. Ryan, C. Negrevergne, M. Laforest, E. Knill, and R. Laflamme, Phys. Rev. A **78**, 012328 (2008).
[34] We have numerically simulated the two experiments with and without the anyonic manipulation. In the simulations we started from different initial states: (1) $|\Psi_f{}'\rangle = |\Psi_a{}'\rangle = |\Psi_{\mathrm{ground}}\rangle$; (2) $|\Psi_f{}'\rangle = |\Psi_a{}'\rangle = |\Psi'_{\mathrm{ground}}\rangle$; (3) $|\Psi_f{}'\rangle = |\Psi_a{}'\rangle = \alpha|\Psi_{\mathrm{ground}}\rangle + \beta|\Psi_{\mathrm{excited}}\rangle$ $(|\frac{\alpha}{\beta}| = 5)$; (4) $|\Psi_f{}'\rangle = |\Psi_a{}'\rangle = \alpha|\Psi_{\mathrm{ground}}\rangle + \gamma|\Psi_{\mathrm{error}}\rangle$ $(|\frac{\alpha}{\gamma}| = 5)$. Here, $|\Psi'_{\mathrm{ground}}\rangle$ is an imperfect ground state which gives rise to two unequal peaks after measurement, $|\Psi'_{\mathrm{ground}}\rangle = \sqrt{\frac{3}{14}}(|000000\rangle + |111000\rangle) + \sqrt{\frac{4}{14}}(|110111\rangle + |001111\rangle)$. The simulation results of η in the above four cases are all about 0.02π, showing that the anyonic braiding process is robust against small errors in the ground-state preparation.
[35] G. M. Leskowitz and L. J. Mueller, Phys. Rev. A **69**, 052302 (2004).